Opto-Electronic Advances

Original Article

2020, Vol. 3, No. 5

DOI: 10.29026/oea.2020.190035

# Omnidirectional iridescence via cylindrically-polarized femtosecond laser processing

Nikolaos Livakas[1,2], Evangelos Skoulas[1,2] and Emmanuel Stratakis[1,3]*

We report the femtosecond (fs) laser fabrication of biomimetic omnidirectional iridescent metallic surfaces exhibiting efficient diffraction for practically any angle of light incidence. Such diffractive behavior is realized by means of multi-directional low-spatial-frequency, laser-induced periodic surface structures (LSFL) formed upon exploiting the cylindrical symmetry of a cylindrical vector (CV) fs field. We particularly demonstrate that the multi-directional gratings formed on stainless steel surface by a radially polarized fs beam, could mimic the omnidirectional structural coloration properties found in some natural species. Accordingly, the fabricated grating structures can spatially disperse the incident light into individual wavelength with high efficiency, exhibiting structural iridescence at all viewing angles. Analytical calculations using the grating equation reproduced the characteristic variation of the vivid colors observed as a function of incident angle. We envisage that our results will significantly contribute to the development of new photonic and light sensing devices.

**Keywords:** laser processing; structural colors; radial polarisation

Livakas N, Skoulas E, Stratakis E. Omnidirectional iridescence via cylindrically-polarized femtosecond laser processing. *Opto-Electron Adv* **3**, 190035 (2020).

## Introduction

A distinct type of coloration found in nature comes as a result of the analysis of the incident light to individual wavelengths realized by sophisticated periodic or pseudoperiodic constructions present within the body of natural species[1]. As a result, the so-called structural colors originate from the fundamental optical processes of diffraction, interference or scattering and exhibit attractive features, including iridescence, angle- and polarization-dependent response. Most important structural coloration is permanent and durable contrary to the pigment coloration, which is sensitive to environmental factors such as heat, UV radiation, and interaction with chemicals. As a consequence, structural colors have attracted significant research interest in the field of biomimetics[2].

Owing to their unique optical properties, bioinspired diffractive surfaces with multiple periodic structures are commonly used as diffracting elements for a plethora of scientific and industrial applications, such as color and holographic displays, telecommunication[3], cosmetics[4], anti-counterfeiting[4–6], spectroscopy and color analysis systems, solar cells[7], and biomedical devices. Structural coloration on technical surfaces is typically achieved by patterning the surface to form gratings exhibiting periodicities on the order of the visible wavelengths. Nowadays, several techniques have been employed to texture materials in the micro- and submicrometer range including electron-beam lithography and etching process[8], or ablation with focused ion beam[9]. Among the mask-free fabrication methods, laser-based direct patterning techniques are proved to be promising for structural coloration, as they are simple and single-step processes[10–12]. In particular, surface processing with pulsed lasers has been used for the manufacturing of submicron periodic structures that appear within the laser beam limits after

[1]Institute of Electronic Structure and Laser, Foundation for Research and Technology-Hellas, Heraklion Crete 71110, Greece. [2]Department of Materials Science and Technology, University of Crete, Heraklion Crete 71003, Greece. [3]Department of Physics, University of Crete, Heraklion Crete 71003, Greece.

*Correspondence: E Stratakis, E-mail: stratak@iesl.forth.gr

Received: 16 September 2019; Accepted: 26 November 2019; Published: 21 May 2020

irradiation[13–17]. In particular, the fabrication of LSFL in the form of parallel fringes with great spatial accuracy and homogeneity are possible upon irradiation with ultrashort laser pulses, due to the limited collateral damage and thermal effects. The formation mechanism of these periodic structures has been investigated by many researchers[18–21]. LSFL are thoroughly characterized by their depth, periodicity, and orientation. Both periodicity and depth are dependent on the fundamental characteristics of the laser irradiation such as wavelength, intensity, and scanning speed[17]. However, their orientation is absolutely dependent on the polarization state of the laser beam[22]. Specifically, for metallic surfaces, LSFL align perpendicularly to the incident net force of the E-field components for a typical linearly polarized pulse[23–26]. Vorobyev and Guo[27,28] have demonstrated the possibility of realizing well-defined structural color via a precise control of periodicity and orientation of LSFL, upon changing various irradiation parameters. Following this work, there are numerous reports on the fabrication of structural colors via laser based fabrication approaches[10–12,29–32,33].

Nevertheless, none of the methods reported to date, including the laser-based ones, is capable to produce multi-directional spatial frequency patterns, in a single step. As a consequence, the produced iridescence strongly depends on the viewing angle, thus it exists only for specific angles of incidence and is absent upon tilting the diffraction element[34,35]. Besides this, it has been both experimentally and theoretically reported, that diffraction cannot occur when the plane of light incidence is parallel to grating orientation[23,36]. Efforts have been made in order to overcome the above restrictions with the generation of LSFL in variable orthogonal directions by utilizing the polarization dependence of the ripple orientation. In particular, a grid can be fabricated where each laser scanning direction employs different polarization state such as p and s polarization respectively[36,37]. Therefore, the surface can produce diffraction in two different planes of incidence. Also, it has recently been reported that irradiation with circular polarization pulses can form triangular periodic surface structures that could potentially significantly increase the range of incident light-illumination angles[38]. Despite these efforts, omnidirectional iridescence has not yet been realized via a single-step irradiation process.

In this paper we present, an effective, simple and single-step technique for the fabrication of diffractive surfaces, exhibiting iridescence with great efficiency for any angle of incidence. This is realized via large-area processing of steel with radially polarized cylindrical vector (CV) fs laser beams[25,39], leading to the formation of LSFL, which are spatially oriented in multiple directions. It is observed that for practically every possible incident angle of illumination, the plane direction of light is always perpendicular to locally formed LSFL, hence reflective diffraction can take place. The ability of the obtained structures to act as diffraction gratings was systematically studied and compared against the diffraction originating on the conventional ones fabricated using linearly polarized laser pulses.

## Materials and methods

Figure 1 shows the laser processing setup used for the fabrication of the two types of surfaces with LSFL structures. In particular, the $S_1$ sample series were fabricated with s-polarized Gaussian beam, while the $S_2$ with radial polarization, at the same irradiation conditions. The main irradiation source was an Yb:KGW laser, emitting 1026 nm linearly polarized pulses of 170 fs duration and 1 kHz repetition rate. The beam was focused on the sample by an achromatic convex lens of 100 mm focal length; the Gaussian spot diameter was ~38 μm at $1/e^2$, measured by a CCD camera on the focal plane. For the generation of a radially polarized CV beam an s-waveplate was placed before the focusing lens[40]. Polished stainless steel (1.4307)

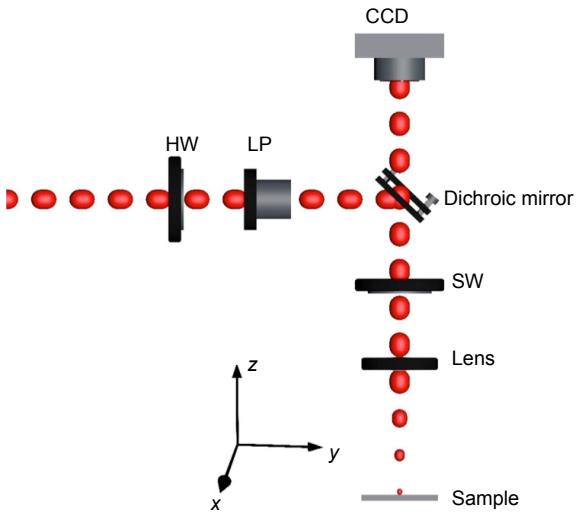


**Fig. 1 | The experimental setup used for surface structuring.** The laser fluence was tuned via the use of a $\lambda/2$ waveplate (HW) and a linear polarizer (LP). Laser source emits a Gaussian linearly polarized beam, which is transformed to a CV radially polarized beam by means of an s-waveplate (SW). Large areas were produced via translation of the sample in the *x*-*y*-*z* directions.

samples were fixed onto a 3-axis motorized stage and positioned perpendicular to the incident beam. All irradiation experiments were performed in ambient conditions. For the systematic study of the processing outcome, both the incident fluence ($F$), as well as the effective number of pulses ($N_{\rm eff}$) should be considered. To calculate the corresponding $F$, in each case, the different spatial intensity profiles of Gaussian and CV beams should be taken into account[41,42]. $N_{\rm eff}$ is the number of laser pulses per unit length or per unit area and for Gaussian beams corresponds to the number of accumulated pulses, which fall upon one-dimensional scanning, onto a length interval equal to the Gaussian beam diameter $2R$. In the case of CV beams, $N_{\rm eff}$ should depend on the corresponding donut-shaped beam area. In general, the effective number of pulses is affected by the scanning velocity, $v$, and thus the repetition rate, $f$. In case of line scanning, the effective pulse number, $N_{\rm eff\text{-}line}$ can be calculated from:

$$N_{\rm eff\text{-}line}=2R\cdot(f/v)\,,\ \text{for Gaussian beam,} \quad (1)$$

$$N_{\rm eff\text{-}line}=2(R-r)\cdot(f/v)\,,\ \text{for CV beam,} \quad (2)$$

where $R$ is the Gaussian beam radius, while for CV beams, $R$ is the outer and $r$ the inner radius. In the case of area scanning at constant velocity $v$, repetition rate $f$ and distance between successive scanning lines ($\delta$), $N_{\rm eff\text{-}area}$ can be calculated from:

$$N_{\rm eff\text{-}area}=\pi R^2\cdot f/(v\cdot\delta)\,,\ \text{for Gaussian beam,} \quad (3)$$

$$N_{\rm eff\text{-}area}=\pi(R-r)^2\cdot f/(v\cdot\delta)\ ,\ \text{for CV beam.} \quad (4)$$

The morphology of the periodic surface structures has been characterized by scanning electron microscopy (SEM, JEOL JSM-7500F). In order to determine the LSFL periodicity and directionality, SEM images were analyzed via two-dimensional fast Fourier transform (2D-FFT), using the Gwyddion software.

To investigate the influence of the angle of an incident white light on the structural color formation, a diffraction characterization setup was built, as shown in Fig. 4. The setup comprises a LED white light source; this light is analyzed in $x$ and $z$ components, with the $x$-component always being at the negative part of the $x$-axis. The angle $\omega$ is defined as the angle between the $x$-axis and the LSFL orientation. For all measurements, the $m$=±1 diffraction orders were taken into account.

## Results and discussion

The generation of LSFL with the best possible uniformity depends strongly on the irradiation parameters. For this purpose, a comprehensive parametric study was conducted via line scanning, to investigate the effect of $F$ and $N_{\rm eff}$ on the topographical features induced. The parametric study led to the creation of optimized, well-organized and uniform LSFL structures under specific irradiation conditions for both polarization states. Figures 2(a) and 2(b) show the calculated periodicities of the optimized LSFL structures obtained for $S_1$ and $S_2$ sample series respectively.

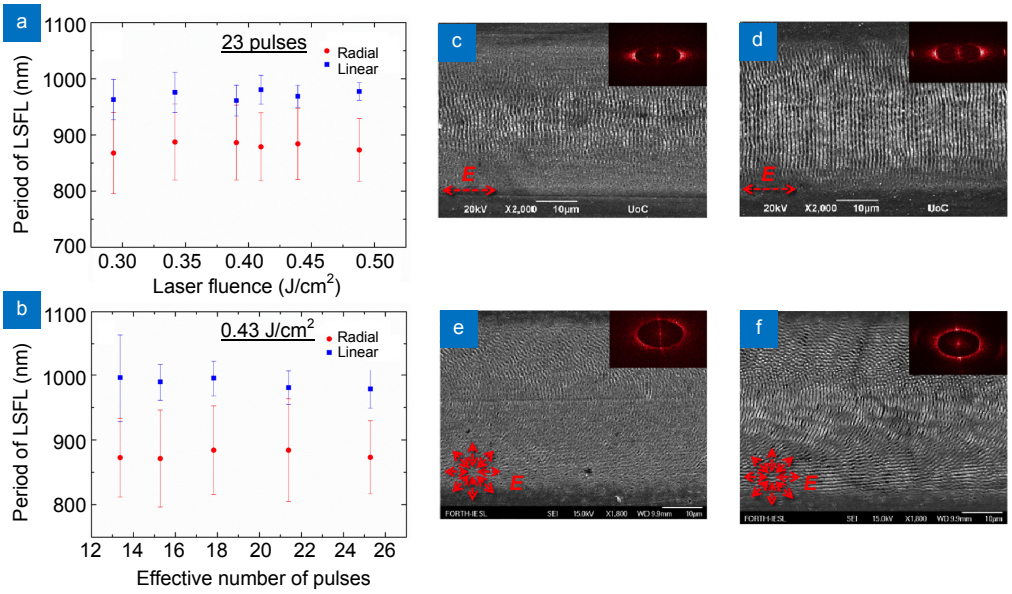


**Fig. 2 | LSFL periodicity dependence on the laser fluence (a), and the effective number of pulses (b), for linearly (squares) and radially (circles) polarized fs beams. Top-view SEM images of areas produced upon irradiation using linearly (c,d) and radially (e,f) polarized fs beams.** The images shown in (c) and (e) correspond to non-uniform areas, whereas those in (d) and (f) to areas obtained using optimized irradiation conditions. The red arrows depict the electric field polarization state. The 2D-FFT patterns corresponding to each area are shown.

It is observed that the LSFL produced via CV beams exhibit lower periodicities, which is in accordance to our former findings and interpretation[25,43]. Furthermore, in both $S_1$ and $S_2$ cases, the periodicity is weakly affected by the laser fluence. Figures 2(c–f) present typical SEM images of non-uniform and optimized areas obtained using linear (c, d) and radial (e, f) polarizations, respectively.

Large areas of 5 mm × 5 mm were also fabricated via scanning the fs beam onto the sample surface using the optimized conditions found during the line scanning experiments. Figures 3(a–c) illustrates the characteristic morphologies attained for the $S_1$ samples, using $F$=0.45 J/cm$^2$, $N_{\text{eff-area}}$=36, $\delta$=32 μm and $v$=2 mm/s. The corresponding 2D-FFT, frequency spectrum, acquired by the SEM images, indicates that the LSFL structures exhibit a single and well-defined directionality, which is perpendicular to the laser beam polarization.

The average period calculated by the FFT pattern for the linear-polarized case equals to 870±80 nm. On the other hand, areal scanning with CV beams gives rise to more complex LSFL structures exhibiting multi-directional orientation (Figs. 3(d–f)). As previously reported[25], such structures are the outcome of the dynamic evolution of the overlap between successive CV beam spots. Indeed, there are two different kinds of overlap taking place in this case. The first is the pulse overlap between successive CV beam spots as the beam advances on the surface during line scan and the second is the overlap between two successive scan lines. In both cases, the crossing of the electric field vectors between successive CV beam pulses determines the LSFL direction per irradiation area. The corresponding 2D-FFT pattern, presented in the inset of Fig. 3(d), shows no dominant spatial frequency, which confirms the multidirectional nature of the formed structures. The average LSFL periodicity calculated in this case equals to 850±97 nm.

Following irradiation, all the processed surfaces exhibited vivid coloration, which is expected, considering that the calculated LSFL periodicities are close to the visible wavelengths[44,45]. It is also striking that the $S_2$ samples are iridescent at practically any viewing angle, contrary to the $S_1$ ones.

Figure 4(a) shows the geometry of the developed optical set up which was used to study the white light diffraction properties of such surfaces, while Fig. 4(b) depicts a typical white light spectrum detected for a specific angle of incidence. Based on the color measuring system, the diffracted light wavelengths can be calculated by the diffraction grating equation[45]

$$m\lambda = \Lambda(\cos\varphi \cdot \sin\omega + \sin\beta) \quad , \tag{5}$$

where $\lambda$ is the diffracted wavelength, $\Lambda$ corresponds to the LSFL period, and $m$ is the order of diffraction, in our case $m$=±1. The angle $\varphi$ denotes the white light incidence, while $\omega$ corresponds to the sample rotation within the sample plane. Assuming that $\theta$ is the sample tilt angle, the grazing angle equals to $\varphi$+$\theta$. The ability of the surface to act as a diffraction grating was tested for eight different angles $\omega$, starting from 0° to 360° with a step of 45°. For each angle $\omega$, the grazing angle was changed accordingly and the corresponding coloration was captured by a camera, placed along the $z$-axis. The angle $\beta$ was also recorded for each measurement.

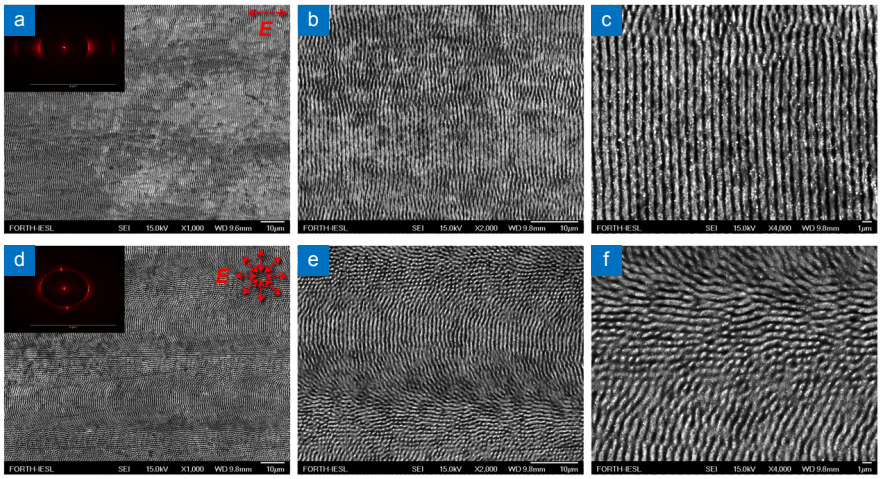


**Fig. 3 | Top-view SEM images of areas produced upon irradiation using linearly (a–c) and radially (d–f) polarized fs beams.** The images shown in (b,c) and (e,f) are higher magnifications of the images (a,d) respectively. The areas in (a–c) were fabricated at $F$=0.45 J/cm$^2$ and $N_{\text{eff-area}}$=36, $\delta$=32 μm, and $v$=2 mm/s, while those in (d–f) were obtained at $F$=0.49 J/cm$^2$, $N_{\text{eff-area}}$=30, $\delta$=34 μm, and $v$=2 mm/s. The red arrows depict the electric field polarization state. The 2D-FFT patterns corresponding to each area are shown in the insets.

Figure 5(a) presents in the form of a polar plot of the angle $\omega$, the structural coloration in the case of the, single spatial frequency, $S_1$, surface, which is in good agreement with the theoretical predictions[44]. Indeed, no diffraction is observed when the ripple orientation becomes parallel to the $x$-axis (i.e. $\omega$=0° and 180°). On the contrary, when the $x$-axis is perpendicular to the ripples orientation, i.e. the angle $\omega$ was 90° and 270°, diffraction with the maximum intensity takes place and vivid structural colors are observed. Diffraction was also occurred for the rest of

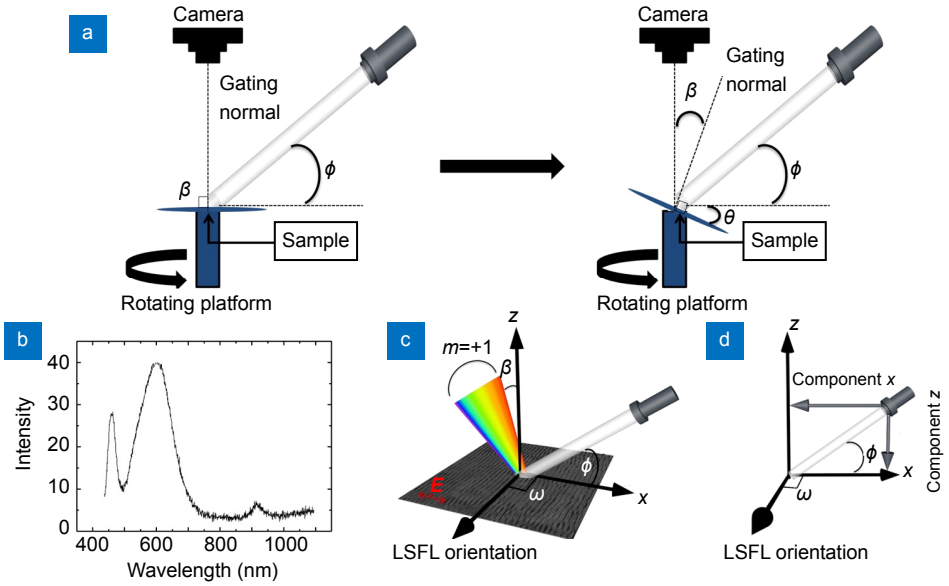


**Fig. 4 |** (**a**) Experimental setup and geometry used for the evaluation of surface diffraction properties. (**b**) Typical intensity plot of the white light spectrum. (**c**) Schematic illustration of the structural color monitoring system. (**d**) The respective coordination parameters.

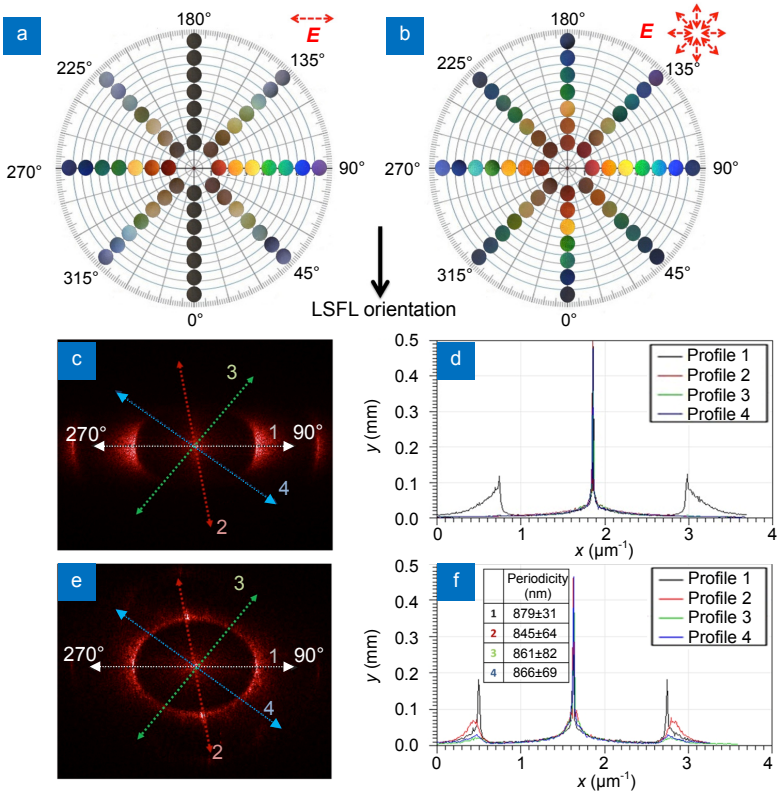


**Fig. 5 | Schematic illustration of the structural colors observed the $S_1$ (a) and the $S_2$ (b) sample series respectively; 2D-FFT patterns corresponding to the $S_1$ (c) and the $S_2$ (e) sample series respectively. The corresponding intensity plots of the 2D-FFT patterns in four different directions (denoted as '1' to '4') are depicted in (d) and (f) respectively.** Inset in (f) displays the periodicity values of LSFL structures for a series of four cross-sections taken in the Fourier image of the $S_2$ surface.

angles $\omega$ tested, i.e. 45°, 135°, 225° and 315°, but with a lower intensity and yield. As a result the structural colors appeared as blurred.

As mentioned above, the diffraction properties and respective structural colors are quite different for the $S_2$ series of surfaces fabricated by a radially polarized CV beam. This is due to the formation of multi-directional LSFL structures, giving rise to reflective diffraction, regardless of the rotational angle $\omega$. As a result, the surface is iridescent for practically any viewing angle, although the vividness and sharpness of the diffracted colors are slightly different depending on the angle $\omega$. Specifically, for the angles $\omega$ = 0°, 90°, 180°, and 270°, the diffracted colors appeared to be most vivid and exhibit the maximum rendering capacity, compared to the angles $\omega$ = 45°, 135°, 225°, and 315°. This effect is also indicated by the respective FFT pattern as shown in Figs. 5(e, f), which shows characteristic hot spots only for the angles where the diffraction is dominant. This inhomogeneity is due to the fact that the pulse overlap does not allow fully homogeneous distribution of the ripple structures attained (i.e. slightly different areal density for every possible direction). Figure 5(f) presents the intensity analysis of the FFT pattern for four different radial directions. In particular, the direction '1' is perpendicular to Gaussian LSFL orientation (i.e. the labeled angles 90° and 270° denote values of angles $\omega$), while the direction '2' is close to the direction parallel to LSFL orientation. It is shown that the higher FFT intensities correspond to the directions '1' and '2' (i.e. $\omega$ = 0°, 90°, 180°, and 270°), while the lower ones to the '3' and '4' (i.e. $\omega$ = 45°, 135°, 225° and 315°) respectively. The average LSFL periodicity, calculated in the four different directions, shown in the inset of Fig. 5(f), confirms that the frequency of the structures remains almost the same and within the standard deviation, regardless of their orientation. Figure 6 also displays analytically all the diffracted colors presented at Figs. 5(a, b) including the exact values of polar ($\omega$), grazing ($\varphi$+$\theta$) and diffracted ($\beta$) angles.

## Conclusions

We have presented a novel technique for the fabrication of large areas of multi-directional laser-induced periodic surface structures exhibiting omnidirectional diffraction properties. It is based on LSFL formed upon exploiting the cylindrical symmetry of CV fs field. The diffraction and structural coloration properties are by far different than those exhibited by LSFL areas fabricated via linearly

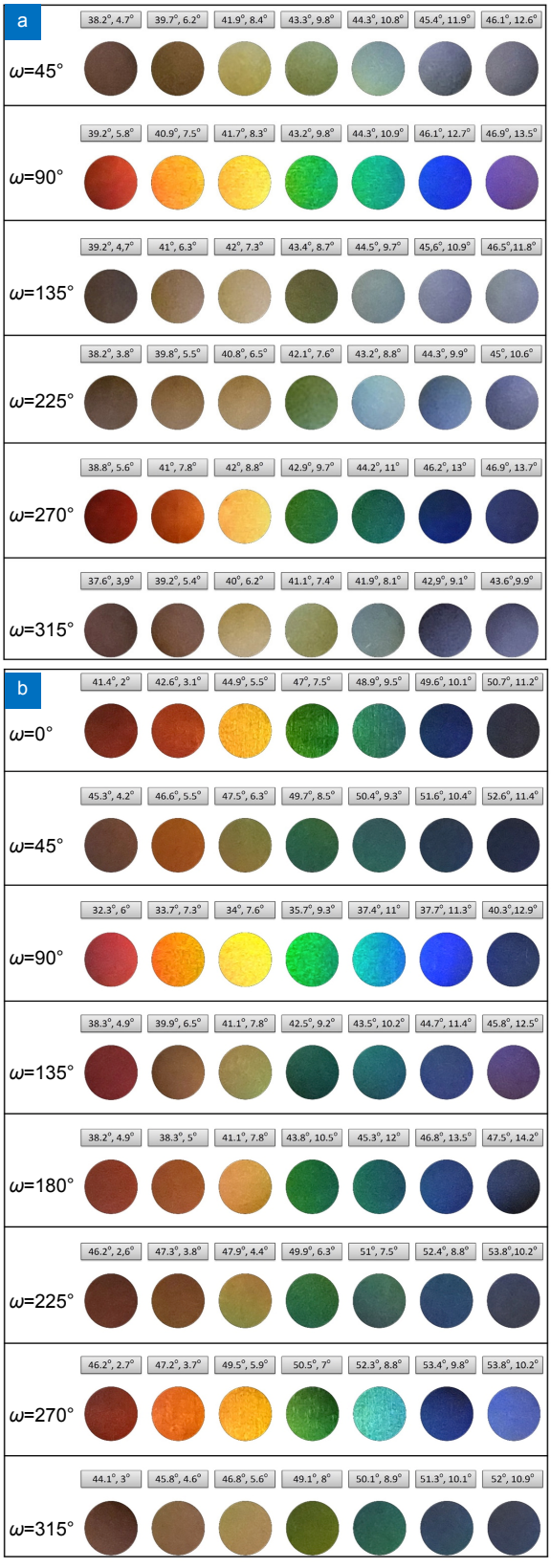


**Fig. 6 |** (**a**) Diffracted colors of $S_1$ surfaces obtained upon irradiation with linearly polarized fs beam. (**b**) Diffracted colors of $S_2$ surfaces obtained upon irradiation with radially polarized fs beam. Each color is characterized by the coordinates ($\omega$, $\varphi$+$\theta$, $\beta$), as defined by the optical system used for their monitoring.

polarized Gaussian beams. Our results show that it is possible to efficiently tune the diffraction and structural coloration properties via surface processing strategies employing femtosecond CV beams. We envisage that this work will pave the way for the realization of customized photonic components and devices.

## References


1. Dumanli A G, Savin T. Recent advances in the biomimicry of structural colours. *Chem Soc Rev* **45**, 6698–6724 (2016).
2. Kumar C S S R. *Biomimetic and Bioinspired Nanomaterials* (Wiley, Weinheim, 2010).
3. Iida M, Hagiwara K, Asakura H. Holographic fourier diffraction gratings with a high diffraction efficiency optimized for optical communication systems. *Appl Opt* **31**, 3015–3019 (1992).
4. Loewen E G, Popov E. *Diffraction Gratings and Applications* (M. Dekker, New York, 1997).
5. Rößler F, Kunze T, Lasagni A F. Fabrication of diffraction based security elements using direct laser interference patterning. *Opt Express* **25**, 22959–22970 (2017).
6. Mahalik N P, Micromanufacturing and nanotechnology. Berlin, Heidelberg: Springer Berlin Heidelberg, 2006.
7. Singh S. Diffraction gratings: aberrations and applications. *Opt Laser Technol* **31**, 195–218 (1999).
8. Saito A, Miyamura Y, Nakajima M, Ishikawa Y Sogo K et al. Reproduction of the *Morpho* blue by nanocasting lithography. *J Vac Sci Technol B* **24**, 3248–3251 (2006).
9. Watanabe K, Hoshino T, Kanda K, Haruyama Y, Matsui S. Brilliant blue observation from a Morpho-butterfly-scale quasi-structure. *Jpn J Appl Phys* **44**, L48–L50 (2005).
10. Dusser B, Sagan Z, Soder H, Faure N, Colombier J P et al. Controlled nanostructrures formation by ultra fast laser pulses for color marking. *Opt Express* **18**, 2913–2924 (2010).
11. Tamamura Y, Miyaji G. Structural coloration of a stainless steel surface with homogeneous nanograting formed by femtosecond laser ablation. *Opt Mater Express* **9**, 2902–2909 (2019).
12. Voisiat B, Wang W, Holzhey M, Lasagni A F. Improving the homogeneity of diffraction based colours by fabricating periodic patterns with gradient spatial period using Direct Laser Interference Patterning. *Sci Rep* **9**, 7801 (2019).
13. Birnbaum M. Semiconductor surface damage produced by Ruby lasers. *J Appl Phys* **36**, 3688–3689 (1965).
14. Clark S E, Emmony D C. Ultraviolet-laser-induced periodic surface structures. *Phys Rev B* **40**, 2031–2041 (1989).
15. Fauchet P M, Siegman A E. Surface ripples on silicon and gallium arsenide under picosecond laser illumination. *Appl Phys Lett* **40**, 824–826 (1982).
16. Vorobyev A Y, Guo C L. Direct femtosecond laser surface nano/microstructuring and its applications. *Laser Photonics Rev* **7**, 385–407 (2013).
17. Papadopoulos A, Skoulas E, Mimidis A, Perrakis G, Kenanakis G et al. Biomimetic Omnidirectional Antireflective Glass via Direct Ultrafast Laser Nanostructuring. *Adv. Mater* **31**, 1901123 (2019).
18. Tsibidis G D, Fotakis C, Stratakis E. From ripples to spikes: a hydrodynamical mechanism to interpret femtosecond laser-induced self-assembled structures. *Phys Rev B* **92**, 041405(R) (2015).
19. Rudenko A, Colombier J P, Itina T E. From random inhomogeneities to periodic nanostructures induced in bulk silica by ultrashort laser. *Phys Rev B* **93**, 075427 (2016).
20. Wang L, Xu B B, Cao X W, Li Q K, Tian W J et al. Competition between subwavelength and deep-subwavelength structures ablated by ultrashort laser pulses. *Optica* **4**, 637–642 (2017).
21. Bonse J, Höhm S, Kirner S V, Rosenfeld A, Krüger J. Laser-induced periodic surface structures—A scientific evergreen. *IEEE J Sel Top Quant Electron* **23**, 9000615 (2017).
22. Öktem B, Pavlov I, Ilday S, Kalaycıoğlu H, Rybak A et al. Nonlinear laser lithography for indefinitely large-area nanostructuring with femtosecond pulses. *Nat Photonics* **7**, 897–901 (2013).
23. Jin Y, Allegre O J, Perrie W, Abrams K, Ouyang J et al. Dynamic modulation of spatially structured polarization fields for real-time control of ultrafast laser-material interactions. *Opt Express* **21**, 25333–25353 (2013).
24. Li G Q, Li J W, Hu Y L, Zhang C C, Li X H et al. Realization of diverse displays for multiple color patterns on metal surfaces. *Appl Surf Sci* **316**, 451–455 (2014).
25. Skoulas E, Manousaki A, Fotakis C, Stratakis E. Biomimetic surface structuring using cylindrical vector femtosecond laser beams. *Sci Rep* **7**, 45114 (2017).
26. Chichkov B N, Momma C, Nolte S, von Alvensleben F, Tünnermann A. Femtosecond, picosecond and nanosecond laser ablation of solids. *Appl Phys A* **63**, 109–115 (1996).
27. Vorobyev A Y, Guo C L. Colorizing metals with femtosecond laser pulses. *Appl Phys Lett* **92**, 041914 (2008).
28. Vorobyev A Y, Guo C L. Spectral and polarization responses of femtosecond laser-induced periodic surface structures on metals. *J Appl Phys* **103**, 043513 (2008).
29. Li G Q, Li J W, Yang L, Li X H, Hu Y L et al. Evolution of aluminum surface irradiated by femtosecond laser pulses with different pulse overlaps. *Appl Surf Sci* **276**, 203–209 (2013).
30. Ionin A A, Kudryashov S I, Makarov S V, Seleznev L V, Sinitsyn D V et al. Femtosecond laser color marking of metal and semiconductor surfaces. *Appl Phys A* **107**, 301–305 (2012).
31. Ahsan M S, Ahmed F, Kim Y G, Lee M S, Jun M B G. Colorizing stainless steel surface by femtosecond laser induced micro/nano-structures. *Appl Surf Sci* **257**, 7771–7777 (2011).
32. Gnilitskyi I, Derrien T J Y, Levy Y, Bulgakova N M, Mocek T, Orazi L. High-speed manufacturing of highly regular femtosecond laser-induced periodic surface structures: physical origin of regularity. *Sci Rep* **7**, 8485 (2017).
33. Wang L, Chen Q D, Cao X W, Buividas R, Wang X W et al. Plasmonic nano-printing: large-area nanoscale energy deposition for efficient surface texturing. *Light: Sci Appl* **6**, e17112 (2017).
34. Højlund-Nielsen E, Weirich J, Nørregaard J, Garnaes J, Mortensen N A et al. Angle-independent structural colors of silicon. *J Nanophotonics* **8**, 083988 (2014).
35. Yetisen A K, Butt H, Mikulchyk T, Ahmed R, Montelongo Y et al. Color-selective 2.5D holograms on large-area flexible substrates for sensing and multilevel security. *Adv Opt Mater* **4**, 1589–1600 (2016).
36. Yao J W, Zhang C Y, Liu H Y, Dai Q F, Wu L J et al. Selective appearance of several laser-induced periodic surface structure patterns on a metal surface using structural colors produced by femtosecond laser pulses. *Appl Surf Sci* **258**, 7625–7632 (2012).
37. Jwad T, Penchev P, Nasrollahi V, Dimov S. Laser induced ripples' gratings with angular periodicity for fabrication of

diffraction holograms. *Appl Surf Sci* **453**, 449–456 (2018).
38. Romano J M, Garcia-Giron A, Penchev P, Dimov S. Triangular laser-induced submicron textures for functionalising stainless steel surfaces. *Appl Surf Sci* **440**, 162–169 (2018).
39. Torres R, Kaempfe T, Delaigue M, Parriaux O, Hönninger C et al. Influence of laser beam polarization on laser micro-machining of molybdenum. *JLMN-J Laser Micro/Nanoeng* **8**, 188–191 (2013).
40. Beresna M, Gecevičius M, Kazansky P G, Gertus T. Radially polarized optical vortex converter created by femtosecond laser nanostructuring of glass. *Appl Phys Lett* **98**, 201101 (2011).
41. Nivas J J J, He S T, Rubano A, Vecchione A, Paparo D et al. Direct femtosecond laser surface structuring with optical vortex beams generated by a q-plate. *Sci Rep* **5**, 17929 (2015).
42. Nivas J J J, He S T, Song Z M, Rubano A, Vecchione A et al. Femtosecond laser surface structuring of silicon with Gaussian and optical vortex beams. *Appl Surf Sci* **418**, 565–571 (2017).
43. Tsibidis G D, Skoulas E, Stratakis E. Ripple formation on nickel irradiated with radially polarized femtosecond beams. *Opt Lett* **40**, 5172–5175 (2015).
44. Hecht E. *Optics* 4th ed (Addison-Wesley, San Francisco, 2001).
45. Palmer C. *Diffraction Grating Handbook* 6th ed (Newport Corporation, Rochester, NY, 2005).

## Acknowledgements:

This work was supported by MouldTex project-H2020-EU.2.1.5.1 (GrantAgreement No. 768705).

## Competing interests

The authors declare no competing financial interests.